## Macromolecules

pubs.acs.org/Macromolecules Article

# Generalized Model of Cooperative Covalent Polymerization: Connecting the Supramolecular Binding Interactions with the Catalytic Behavior

<sup>4</sup> Hailin Fu,<sup>§</sup> Ryan Baumgartner,<sup>§</sup> Ziyuan Song,<sup>§</sup> Chongyi Chen, Jianjun Cheng,\* and Yao Lin\*



Cite This: https://doi.org/10.1021/acs.macromol.1c02606



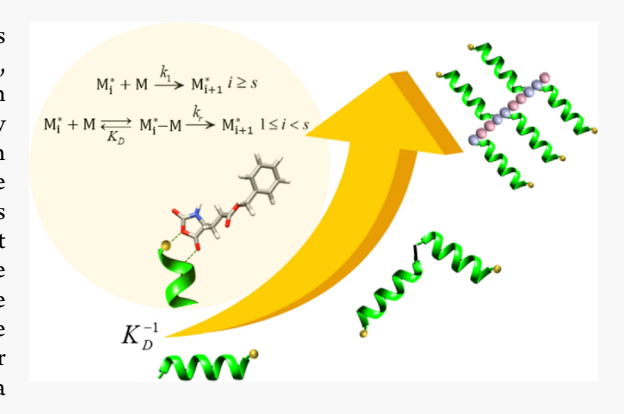
ACCESS

Metrics & More

Article Recommendations

Supporting Information

5 ABSTRACT: The dynamic assembly of actin and tubulin microfilaments 6 from their subunits is imperative in enabling cell motility, cell division, 7 and organismal muscle function. The nucleation-controlled growth 8 kinetics that characterizes these protein polymerizations is facilitated by 9 the cooperative and reversible noncovalent interactions of protein 10 subunits. Although this growth kinetics has been realized in the 11 supramolecular polymerization of numerous synthetic molecules, it is 12 rare in covalent polymerizations since a cooperative binding event 13 between a monomer and a polymer must also lead to catalysis of the 14 polymerization. The ring-opening polymerization of N-carboxyanhydride 15 monomers is one such system that has been shown to result in large 16 degrees of cooperativity and self-acceleration depending on the polymer 17 architecture. Herein, we apply recent experimental data to introduce a 18 simple and generalized kinetic model of cooperative covalent polymer



19 izations, incorporating a Michaelis—Menten-like equation into the rate laws to describe the binding of a monomer to the growing 20 polymer chain explicitly. The treatment of the growing polymer chain as both a cooperative system and as a primitive "enzyme" with 21 a distinct binding event not only increases the applicability of the model but also reduces the number of variables used to describe 22 the system. The theoretical predictions are compared to experimental data with various levels of cooperativity. The application of 23 this simple kinetic model across a broad range of macromolecular architectures with varying levels of cooperativity will help polymer 24 chemists to discover similar mechanisms in nonpolypeptide systems and utilize them to create covalent analogues of natural 25 cooperative systems. The model can be extended to cover a variety of cases in which additional intermediates or competitive 26 reactants occur in the reaction pathway of cooperative covalent polymerization.

#### 27 INTRODUCTION

28 Supramolecular interactions are leveraged by cells to catalyze 29 chemical reactions essential for life including protein synthesis 30 in ribosomes and the polymerization of cytoskeletal 31 filaments. 1-8 These processes rely on a series of binding events and interactions that result in the structural changes of 33 biomacromolecules to a more active state or the colocalization 34 of biomolecules to vastly increase their local concentrations. <sup>9,10</sup> 35 These cooperative supramolecular interactions act to greatly 36 increase the rates of chemical reactions and have been utilized 37 in a variety of synthetic polymerization processes, most often 38 noncovalent, 11-22 but more recently in covalent systems. 23-2639 One such covalent system identified early on by Doty and 40 others is the synthesis of helical polypeptides such as poly( $\gamma$ -41 benzyl-L-glutamate) (PBLG) via the ring-opening polymer-42 ization (ROP) of amino acid N-carboxyanhydrides 43 (NCAs). 27-29 The reaction proceeds with a primary amine-44 based initiator to open the ring of the NCA monomer. 45 Subsequent decarboxylation of the resulting structure results in 46 the addition of a single amino acid to the growing polymer chain and the recovery of the active amine. In specific solvents, 47 this polymerization was characterized by slow chain 48 propagation, followed by a modest but distinct acceleration 49 in a second stage that took place once  $\alpha$ -helices could be 50 stabilized in a solution [the degree of polymerization (DP) of 51 6-10]. Thrigued by the unusual cooperative behavior in 52 this polymerization, we recently discovered that very strong 53 cooperative effects can be induced in various macromolecular 54 and supramolecular architectures that promote colocalization 55 and polymer–monomer interactions to drastically accelerate 56 the polymerization of NCAs into helical polypeptides. The polymerization of NCAs into helical polypeptides are polypeptides. The polymerization of NCAs into helical polypeptides are polypeptides. The polymerization of NCAs into helical polypeptides are polypeptides are polypeptides. The polypeptides are polypeptides are polypeptides are polypeptides are polypeptides. The polypeptides are polypeptides are polypeptides are polypeptides are polypeptides are polypeptides.

Received: December 22, 2021 Revised: February 4, 2022



(a) (b) (c) 
$$I+M \xrightarrow{k_1} M_1^{\epsilon} \qquad I+M \xrightarrow{k_1} M_1^{\epsilon}$$
 
$$I+M \xrightarrow{k_1} M_{i+1} \qquad 1 \le i < s \qquad M_i^{\epsilon} + M \xrightarrow{k_1} M_{i+1} \qquad 1 \le i < s \qquad M_i^{\epsilon} + M \xrightarrow{k_1} M_{i+1} \qquad 1 \le i < s$$
 
$$M_i + M \xrightarrow{k_2} M_{i+1} \qquad i \ge s \qquad M_i^{\epsilon} + M \xrightarrow{k_2} M_{i+1} \qquad i \ge s \qquad M_i^{\epsilon} + M \xrightarrow{k_{max}} M_i^{\epsilon} - M \xrightarrow{k_m} M_{i+1} \qquad i \ge s$$

60 in modeling the two-stage kinetic profiles in the NCA-ROP 61 (Figure 1b) across various polymer architectures. 23-25

Recently, with nuclear magnetic resonance (NMR)-based 63 experiments and molecular dynamics simulations, we eluci-64 dated that the auto-acceleration in NCA polymerizations is due 65 to monomer binding to the actively growing N-terminus of  $\alpha$ -66 helical polypeptides in the elongation stage (Figure 1c). This 67 mechanism is not unlike the classical Michaelis-Menten (MM)-type kinetics that describes enzymatic systems in which distinct binding event of the substrate to the active site 70 occurs. 30,31 Realizing that  $\alpha$ -helical polypeptides may be 71 treated as catalytic pseudo-species in the chain propagation 72 reaction is important, as we can now examine across various 73 macromolecular architectures by focusing on the factors that 74 promote the "polymer-monomer" interactions to gain further 75 insight into the widely different cooperative strengths observed 76 in the auto-accelerated polymerization kinetics. Here, we 77 consider this reversible binding event between the NCA 78 monomers and the growing helical chains and introduce a 79 generalized treatment of the cooperative covalent polymer-80 ization by approximating the rate laws for accelerated chain 81 elongation explicitly using a MM-like equation. This approach 82 reduces the number of parameters in the model and allows for 83 potential extensions and modifications of the kinetic frame-84 work for autocatalytic polymerizations in general. The model 85 can interpret the existing kinetic phenomena in ROP-NCAs 86 obtained with various levels of cooperativity. The different 87 cooperative strengths are simply quantified by the effective 88 binding affinity in the model. The unified theoretical 89 framework and experimental strategy presented here should 90 accelerate the discovery of novel reaction systems that 91 incorporate strong cooperative effects for the controlled 92 synthesis of polymers.

#### 93 THEORETICAL BASIS

Oosawa-MM Model of Cooperative Covalent Polymerization. Previously, we have shown that NCA monomers undergo reversible adsorption/desorption to the active polymerization site of the helical polypeptide prior to the irreversible ring-opening of the NCA monomer. To describe this, a two-staged, Oosawa-type kinetic model was established with the monomer adsorption step incorporated into the

elongation stage, as described by the successive reactions in 101 Figure 1c, where M represents monomer and Mi\* denotes a 102 polymer chain with a DP of i and an active site (\*) at the end. 103 In the initial stage of the chain growth where the DP of i is less 104 than the critical chain length (s, the nucleus for helix 105 formation), we treated the reaction between the monomer 106 and the active end of the coil chain as a second-order reaction 107 with a rate constant  $k_1$ . When  $i \ge s$ , the propagation rate 108 increases due to cooperative interactions stemming from the 109 formation of the  $\alpha$ -helix. In this accelerated elongation stage, 110 we considered the reaction to occur in two steps: first, the 111 monomer binds to the active helical chain to form the reaction 112 complex  $M_i^* - M_i$ , with an adsorption rate constant  $k_{on}$  and a 113 desorption rate constant  $k_{\rm off}$ ; subsequently, the attack of the 114 active end of the helical chain on the bound monomer triggers 115 a ring-opening reaction and allows for the chain elongation 116 with a rate constant  $k_r$ . Based on this model, it was then 117 standard practice to write the concentration flux equations<sup>20</sup> 118 (Figure S1) corresponding to the abovementioned scheme and 119 determine their numerical solutions.

Although the concentration flux approach explicitly 121 describes the microscopic processes of chain growth, the 122 adsorption and desorption rate constants ( $k_{\rm on}$  and  $k_{\rm off}$ ) 123 respectively) cannot be individually determined with good 124 accuracy, and usually it takes more iterations of numerical 125 solutions to avoid local minima and find the best estimates of 126 kinetic parameters from experimental data in comparison with 127 the phenomenological model<sup>23</sup> shown in Figure 1b. Here, we 128 describe a simple rate equation system by focusing on the time 129 evolution of the principal moments: the mass concentration 130 m(t) (or the concentration of polymerized monomers) and the 131 number concentration P(t) of the polymers

$$m(t) = \sum_{i=s}^{\infty} iM_i(t),$$
  $P(t) = \sum_{i=s}^{\infty} M_i(t)$ 

and by incorporating the MM equation explicitly into the 133 differential rate equations. Following the convention in 134 cooperative supramolecular polymerization, we include in P 135 any chains longer than the nucleus  $(i \ge s)$ . The two quantities, 136 m(t) and P(t), are experimentally most accessible, for example, 137 by monitoring the monomer consumption in the reaction 138

139 through spectroscopic methods. Their quotient m(t)/P(t), 140 gives the average length of the polymer DP, and can be verified 141 by measuring the molecular weight (MW) of resulting 142 polymers by gel permeation chromatography (GPC) or other 143 standard methods.

The two-step reaction in the elongation stage is analogous to an enzymatic reaction described by MM-type kinetics in which the actively growing chain end acts as the "enzyme" and the monomer is the "substrate". A reversible bimolecular binding occurs first between the growing chain and the monomer, followed by an irreversible unimolecular reaction that incorporates the bound monomer covalently into the chain and recovers the number of active chain ends. Under a quasi-steady-state assumption that generally holds for this type of catalytic polymerization, the rate equation of polymerized monomers can be described by the MM-type equation

$$\frac{\mathrm{d}m(t)}{\mathrm{d}t} = \frac{k_{\mathrm{r}}M(t)P(t)}{K_{\mathrm{D}} + M(t)} \tag{1}$$

156 where  $K_{\rm D}$  is the equilibrium dissociation constant of 157 monomers from the growing chain end  $(K_{\rm D}=k_{\rm off}/k_{\rm on})$ , a 158 catalytic pseudo-species acting like an enzyme in the MM 159 mechanism. The differential equation describing the time 160 evolution of monomer concentration M(t) then follows

$$-\frac{dM(t)}{dt} = k_1 M(t) (I_0 - P(t)) + \frac{dm(t)}{dt}$$
 (2)

162 where the first term is the rate of monomer consumption 163 caused by the active chains being shorter than the critical 164 length s, and  $I_0$  is the concentration of initiators at time zero. 165 The kinetic equation for the number concentration of 166 polymers P(t) follows

$$\frac{dP(t)}{dt} = k_1 M_{s-1}(t) M(t)$$
(3)

168 where  $M_{s-1}(t)$  represents the concentration of active chains 169  $(M_{s-1}^*)$  with the length of s-1 at time t and can be obtained 170 by solving

$$\frac{\mathrm{d}M_{i}(t)}{\mathrm{d}t} = k_{1}M(t)(M_{i-1}(t) - M_{i}(t)) \qquad 1 < i < s$$
(4)

$$\frac{dM_{1}(t)}{dt} = -k_{1}M(t)M_{1}(t)$$
(5)

173 and we usually assume  $M_1(0) = I_0$  for fast initiation reaction. 174 Equations 1-5 establish the complete set of differential 175 equations that incorporate the MM equation into the 176 Oosawa–MM (OMM) model for numerical solutions.

In comparison with the model based on concentration flux requations, the fitting parameters of this model have now been reduced from five to four: s,  $k_1$ ,  $k_r$ , and  $K_{\rm D}$ . This allows for the determination of the unique set of fitting parameters by rather carrying out model-based analysis, even with a limited set of set into the rate equation, incorporating the MM-like equation and modification of the kinetic model for two-stage catalytic polymerizations in general. The MM equation holds for many mechanisms, even though the MM mechanism (e.g.,  $k_{\rm r} \ll k_{\rm off}$ ) resonant rather covariety of cases, for example, when  $k_{\rm r}$  is comparable to the set of the single set of the single set of the set of the

on the reaction pathway.  $^{32,33}$  In most cases, the MM equation 191 still applies, although  $K_{\rm D}$  and  $k_{\rm r}$  should be replaced by  $K_{\rm M}$  and 192  $k_{\rm cat}$ , which are combinations of various rate and equilibrium 193 constants (e.g.,  $K_{\rm M}=K_{\rm D}+\frac{k_{\rm r}}{k_{\rm on}}$  in Briggs—Haldane kinetics). 194 In this context, the rate equation for polymerized monomers 195 can be generalized to

$$\frac{\mathrm{d}m(t)}{\mathrm{d}t} = \frac{k_{\mathrm{cat}}M(t)P(t)}{K_{\mathrm{M}} + M(t)} \tag{6}$$

while other rate equations remain the same. The adaptability of 198 this generalized kinetic model is crucial for the discovery of 199 new reaction systems that incorporate different or currently 200 unknown cooperative behaviors into the growth of polymer 201 chains. Major variables and parameters used in the OMM 202 model are listed in Table 1 for quick reference.

Table 1. List of Symbols Used in the OMM Model of Cooperative Covalent Polymerization

symbol	property		
S	critical chain length		
$k_{i}$	initiation rate constant		
$k_1$	second-order rate constant for the first (nucleation) stage of polymerization		
$K_{\mathrm{D}}$	dissociation constant of the noncovalently bound complex from the monomer and the growing chain end in the second(propagation) stage of polymerization		
$k_{ m r}$	first-order rate constant of chain elongation reaction from the noncovalently bound complex		
$\sigma^{-1}$	reciprocal of kinetic cooperativity factor, $\sigma^{-1} = k_{\rm r}/(K_{\rm D}k_{\rm 1})$		
$I_0$	initiator concentration		
$M_0$	monomer concentration		
$K_{\mathrm{M}}$	apparent dissociation constant of the Michaelis complex, $K_{\rm D}$ is replaced by $K_{\rm M}$ in the generalized OMM model to hold for complex reaction mechanisms		
$k_{\rm cat}$	apparent first-order rate constant for the chemical conversion from the Michaelis complex, $k_{\rm r}$ is replaced by $k_{\rm cat}$ in the generalized OMM model to hold for complex reaction mechanisms		

Binding Equilibrium Facilities a Saturation Effect on 204 the Chain Growth Kinetics. In cooperative supramolecular 205 polymerization, the kinetic cooperativity factor  $(\sigma)$  is defined 206 as  $\sigma^{-1} = k_2/k_1$  (Figure 1a), where a large value of  $\sigma^{-1}$  implies a 207 higher cooperativity and  $\sigma^{-1} = 1$  implies no cooperativity. 208 Similarly, the kinetic cooperativity factor for OMM-type 209 cooperative covalent polymerization can be approximately 210 defined as  $\sigma^{-1} = k_r/(K_D k_1)$ . For a system with a defined critical 211 chain length, s, the shape of polymerization kinetics is mainly 212 controlled by the cooperativity factor and the initial 213 monomer-initiator ratio  $(M_0/I_0)$ . Solving the differential eqs 214 1-5 numerically for different  $\sigma^{-1}$  and  $M_0/I_0$  yields the various 215 kinetic curves shown in Figure 2a,b, where the fraction of 216 f2 polymerized monomers is plotted against dimensionless time au 217 =  $tk_1M_0$ . It is not surprising that an enzyme-like saturation 218 effect against increasing  $\sigma^{-1}$  is clearly evidenced in the 219 accelerated propagation stage. In addition, binding equilibrium 220 between monomers and the growing helical chains introduces 221 the terms that explicitly depend on  $M_0$  in the differential 222 equations (see the equations in dimensionless form in Figure 223 S2). Figure 2c shows the predicted kinetic curves from solving 224 eqs 1-5 numerically for an identical set of s, rate and 225 equilibrium constants, and  $M_0/I_0$ , but with different  $M_0$ . 226 Increasing  $M_0$  changes the shape of the kinetic profile even in 227 the dimensionless form (inset of Figure 2c), which contrasts 228

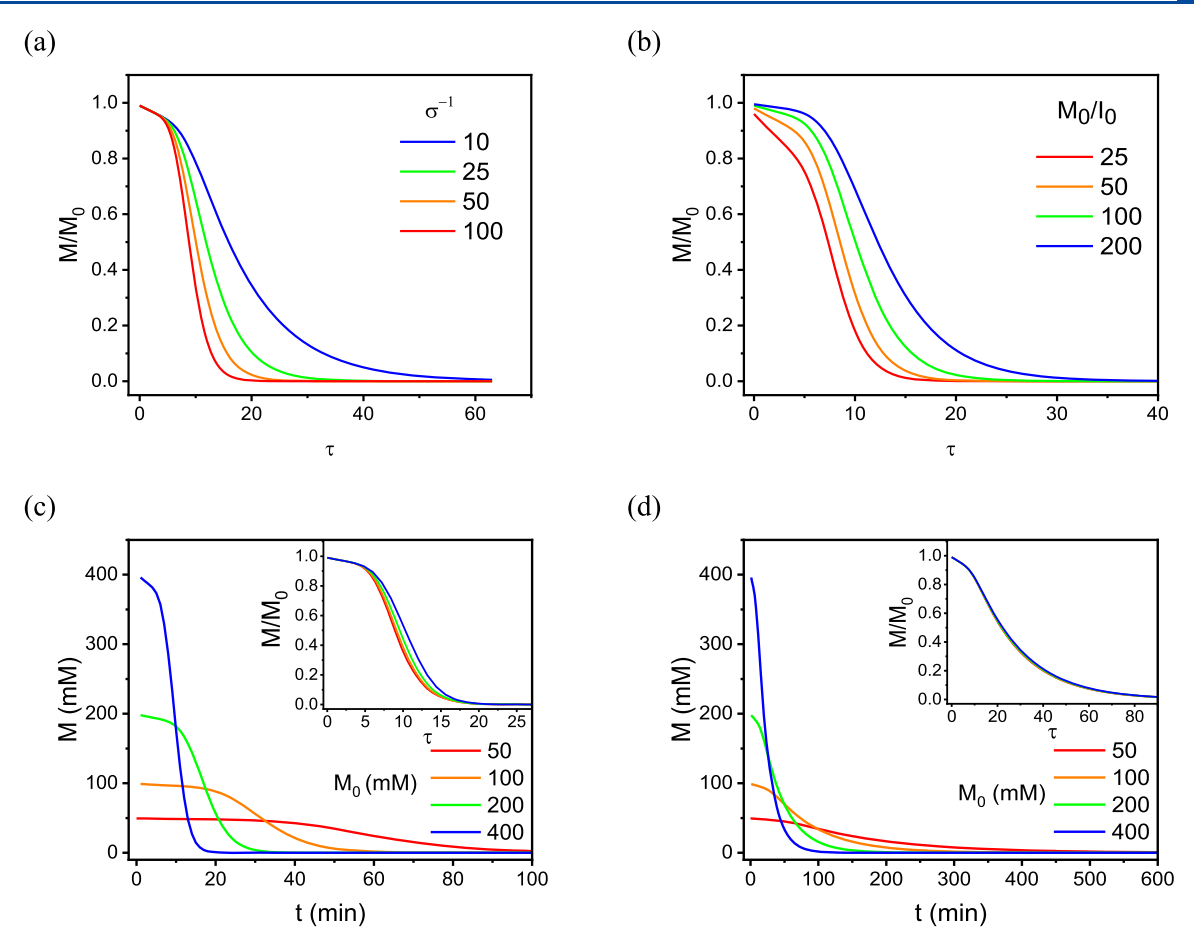


Figure 2. Simulations with the OMM model of cooperative covalent polymerization. (a,b) Plots of the fraction of the monomer versus rescale time  $(\tau = tk_1M_0)$  for test cases with s = 10,  $k_1 = 0.05$  M $^{-1}$  s $^{-1}$ ,  $k_r = 1$  s $^{-1}$ , and  $M_0/I_0 = 100$ , at selected values of  $\sigma^{-1}$  (a), and s = 10,  $k_1 = 0.05$  M $^{-1}$  s $^{-1}$ ,  $k_r = 1$  s $^{-1}$ , and  $\sigma^{-1} = 50$ , at selected values of  $M_0/I_0$  (b). The shape of the curve is heavily influenced by  $\sigma^{-1}$  and the  $M_0/I_0$  ratio. (c) Plots of the monomer concentration vs time for test cases with s = 10,  $k_1 = 0.05$  M $^{-1}$  s $^{-1}$ ,  $k_r = 1$  s $^{-1}$ ,  $k_D = 0.25$  M, and  $M_0/I_0 = 100$ , at selected values of  $M_0$ . The inset shows the plot of the fraction of the monomer vs rescale time for the same condition. (d) Same as (c), but  $K_D = 4$  M. The difference in  $K_D$  changes  $\sigma^{-1}$  from 80 in (c) to 5 in (d). The inset shows that the concentration dependence of kinetic profiles in the dimensionless form almost vanishes.

229 with the prediction of the earlier phenomenological model. <sup>23</sup> The dependence on the monomer concentration reaches 231 saturation when  $M_0$  is far above  $K_{\rm D}$ . Figure S3a shows how the 232 DP of the resulting polymers compares with  $M_0/I_0$  (DP\*) 233 based on the kinetic curves in Figure 2c. In the limit that  $\sigma^{-1}$  234 tends to 1, the concentration dependence of kinetic profiles 235 vanishes and DP/DP\* tends to 1 (Figures 2d and S3b), where 236 eventually single-stage kinetics are recovered. The substantial 237 dependence of kinetic curves and DPs on  $M_0$  is a characteristic 238 of the OMM kinetic model and is clearly evidenced in the 239 experiments.

This exercise also indicates that the elucidation of the 241 catalytic nature of cooperative covalent polymerizations often 242 requires a "global" analysis of the kinetic profiles collected from 243 a series of experiments with different  $M_0$ . This has become a 244 routine practice in the study of supramolecular polymerization; 245 however, it is usually not carried out in covalent polymer-246 ization. Besides, a good choice of  $M_0$  range (to span the 247 saturating region) is important to obtain a reliable outcome 248 from the model-based analysis. At concentrations far above the 249 saturation concentration,  $K_D$  cannot be determined. At 250 concentrations much lower than the saturation concentration, 251 the accuracy in determining  $K_D$  is relatively poor. In the next 252 section, we demonstrate the analysis of two-stage kinetic

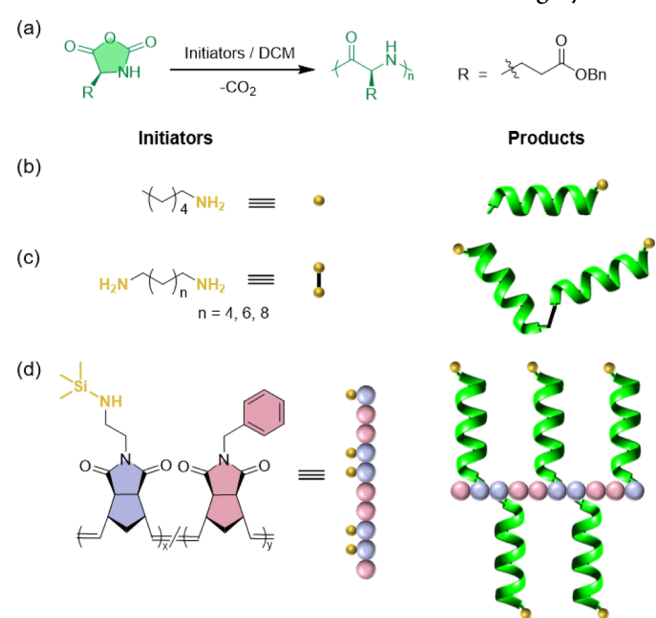
profiles from the ROP-NCA of helical polypeptides under 253 different cooperative strengths. We show that the generalized 254 OMM model can correctly account for the course of monomer 255 consumption over time as observed in the experimental data, 256 and the corresponding trend of the average DP of the 257 polymers.

#### RESULTS AND DISCUSSION

**Experimental Setup of ROP-NCA Kinetics and** 260 **Polypeptide Characterization.** Currently, many experimen- 261 tal studies on cooperative covalent polymerization are based on 262 the polymerization of the γ-benzyl-L-glutamate NCA (BLG- 263 NCA), mainly due to the facile synthesis and purification, the 264 excellent solubility of the monomer and the resulting 265 polypeptide, PBLG (Scheme 1a), and the characteristic coil- 266 s1 to-helix transition during the polymerization. The polymerization kinetics used in this study and the MW distribution 268 (MWD) profiles of the resulting polymers were obtained from 269 our previous published work and new experiments (see the 270 Supporting Information). Profiles and new experiments (see the 271 infrared spectroscopy or proton NMR spectroscopy were 272 used to monitor the disappearance of signals from NCA 273 monomers, which, after normalization, indicated the extent of 274 polymerization in a quantitative manner. Specifically, the 275

259

#### Scheme 1. ROP of NCA with Different Initiating Systems<sup>a</sup>



"(a) Chemical structures of BLG-NCA monomers and PBLG polypeptides. (b-d) Chemical structures of the (macro)initiators and schematic illustration of the corresponding polypeptides grown from the (macro)initiators. Three initiating systems with increasing density of initiating sites were evaluated: a homopolymerization system initiated by n-hexylamine (b), a "hinged" polymerization system initiated by diaminoalkane (c), and a brush-like polymerization system initiated by a poly(NB) bearing pendant trimethylsilylamino side chains (d).

276 polymerization kinetics of three different initiating systems 277 were collected, with increasing density of initiating sites: a low-278 cooperativity system using n-hexylamine as the initiator 279 (Scheme 1b), a medium-cooperativity system initiated from 280 three diaminoalkane (1,6-diaminohexane, 1,8-diaminooctane, 281 and 1,10-diaminodecane, named as  $C_6$ -diNH<sub>2</sub>,  $C_8$ -diNH<sub>2</sub>, and 282  $C_{10}$ -diNH<sub>2</sub>, respectively, in Scheme 1c), and a high-283 cooperativity system with poly(norbornene) [poly(NB)] 284 bearing pendant trimethylsilylamino side chains as the brush-285 like macroinitiator (Scheme 1d).

Polymerization of Helical Homopolypeptides at Low 286 287 Cooperative Strength. We first used the new generalized 288 OMM model to analyze the linear, self-catalyzed polymerization of Glu-NCAs initiated by primary amines into helical 290 PBLG in dichloromethane (DCM). This two-stage, autoaccelerated polymerization in solvents of low dielectric constant proceeds with reversible NCA binding and the 293 subsequent irreversible ring-opening reaction of the NCA 294 monomer. The 27 kinetic profiles collected from three initial 295 monomer concentrations, each with three different  $M_0/I_0$ 296 ratios, and three replicates per condition, 26 were fitted by 297 solving the differential rate eqs 1-5 numerically (Figure 3a-298 c). A global fit was obtained for 27 sets of kinetic data by 299 sharing the same s and  $k_r$  (s = 10 and  $k_r$  = 0.4 s<sup>-1</sup>), while 300 allowing  $k_1$  and  $K_D$  to be optimized for 9 individual conditions. 301 The MWs predicted by the kinetic model based on the 302 optimized parameters are in good agreement with the GPC 303 results from the polymers (Table S1). Figure 3d indicates an 304 interesting correlation between  $k_1$  and  $K_D$  with  $I_0$  (the 305 concentration of active chains), even though the difference 306 in  $k_1$  is rather small. In the nucleation stage  $(k_1)$ , the presence

of short, coil-like chains in which NCA monomers can undergo 307 nonproductive binding with amide groups may interfere with 308 desired binding at the N-terminus. The effect is more 309 pronounced with fewer chains in the solution and may cause 310 the modest decrease of  $k_1$  with lower  $I_0$ . The effect, however, 311 should not play an important role during the fast propagation 312 stage, as the formation of helices with an intrachain H-bonding 313 network prevents NCAs from binding nonspecifically. It is 314 known that the increasing concentration of PBLGs in DCM or 315 chloroform may facilitate some bundling of the helices in the 316 solution, which explains the increase of binding equilibrium 317 constants with  $I_0$  due to a higher "effective concentration" of 318 initiator sites. The effect is more clearly revealed in the 319 polymerization of hinged polypeptide systems (vide infra), in 320 which two growing chains are covalently connected by a 321 synthetic linker.

Polymerization of "Hinged" Polypeptides at Medium 323 Cooperative Strength. When linear aliphatic diamines are 324 used as initiators for the synthesis of helical polypeptides, the 325 polymerization leads to the formation of "hinged" polypeptides 326 in which two chains are grown connected through the flexible 327 diamine initiator. The reaction again follows a two-stage, 328 nucleation-controlled polymerization kinetics, with the accel- 329 eration more than 30-fold faster than that in the polymer- 330 ization of a single isolated polypeptide chain.<sup>24</sup> Having two 331 growing helical chains connected by a linker affects the binding 332 interactions between monomers and the active ends, due to the 333 effect of "local" concentration. We examined the polymer- 334 ization initiated by three different linkers with various spacer 335 lengths (C<sub>6</sub>-diNH<sub>2</sub>, C<sub>8</sub>-diNH<sub>2</sub>, and C<sub>10</sub>-diNH<sub>2</sub>), each at three 336 different  $M_0$  (0.05, 0.10, and 0.15 M, respectively), while 337 keeping  $M_0/I_0$  identical. By sharing the same  $k_{\rm r}$  and s globally, 338 the same  $K_D$  for each type of linker, but allowing  $k_1$  to be 339 individually optimized, a global fit was obtained for nine sets of 340 kinetic data with varying  $M_0$  and  $I_0$  (Figure 4a-c). Such as in 341 f4 the polymerization of homo-PBLG,  $k_1$  increases slightly with  $I_0$  342 for the same spacer (Figure 4d).  $K_D$  is independent of  $I_0$  but is 343 a function of the length of the spacer. The MWs predicted by 344 the kinetic model based on the optimized parameters are in 345 good agreement with the GPC results from the polymers as 346 well (Table S2 and Figure S4). By linking two active growing 347 sites in the proximity, the effective binding affinity of NCA to 348 the helical chains increases by 20-50 fold, depending on the 349 diamine spacer length. The increase in the effective binding 350 coefficient may arise from two effects. The first effect is due to 351 the higher local concentration of initiating sites  $(Mi^*)$  and the 352 second is due to the higher local concentration of the NCA 353 monomer (M). The first effect stems from the diamine linker, 354 which brings initiating sites into proximity to one another. The 355 second is due to the colocalization of monomers, as monomers 356 bound to one helix may react with the active end of the other 357 helix in the same macromolecules. Proximity and colocalization 358 are powerful forces used in biology to accelerate reactions, for 359 instance, in protein allostery. This effect of colocalization on 360 effective binding is large and is also evidenced in the first stage 361 of polymer growth, as  $k_1$  shows a similar dependence on the 362spacer length (Figure 4d). This suggests that the proximity of 363 two active chains can also enhance the interaction of NCA 364 with the shorter chains in their coil state. In practice, however, 365 it is difficult to separate the adsorption term explicitly from the 366 rate constant in the nucleation stage, and it is also unnecessary, 367 as  $k_1$  can be determined with high accuracy from the kinetic 368 profiles. Again, the OMM model functions very well to predict 369

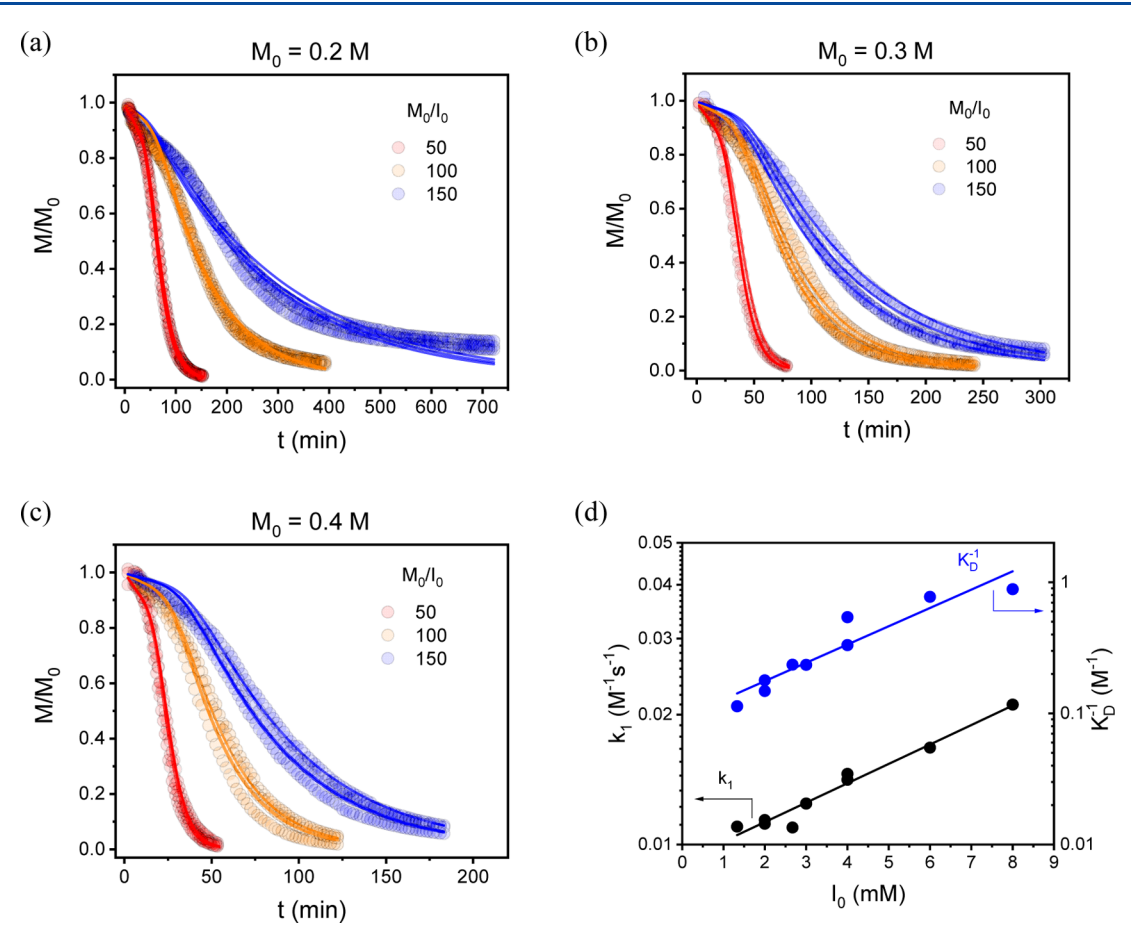


Figure 3. Analysis of self-catalyzed polymerization of helical polypeptides with the OMM model. (a—c) Polymerization kinetics of BLG-NCA in DCM was initiated by hexylamine with  $M_0 = 0.2$  (a), 0.3 (b), and 0.4 M (c). Three  $M_0/I_0$  ratios (50, 100, and 150) were tested for each  $M_0$ , each with three replicates. The kinetic data (circles) is fit with the OMM model (solid lines) by sharing the same s and  $k_r$  (s = 10 and  $k_r = 0.4$  s<sup>-1</sup>) for all the 27 profiles, while allowing  $k_1$  and  $K_D$  to be optimized for 9 individual conditions. (d) Extracted rate constants for the nucleation stage ( $k_1$ ) and the association equilibrium constant ( $K_D^{-1}$ ) from (a—c). The results show an increase of  $k_1$  and  $K_D^{-1}$  with increasing initiator concentration  $I_0$ , possibly due to the existence of some segregation of polymers in the solution.

370 the kinetic profiles of cooperative systems of moderate 371 strength.

Polymerization of Brush-Like Polypeptides at Strong 373 Cooperative Strength. One of the fastest self-acceleration of 374 NCA polymerizations was found in a brush-like polymer 375 system that consists of a linear poly(NB) scaffold containing a 376 high density of initiating groups from which polypeptide chains 377 are grown.<sup>23</sup> NCAs condense on to the initiation sites along 378 the polymeric scaffold to form polypeptide chains, which fold 379 into  $\alpha$ -helices upon reaching a critical chain length ( $s \sim 10$ ). 380 The rate of acceleration was drastic (up to 1000-fold), and was 381 shown to be regulated according to the grafting density (f) of 382 initiators on the polymeric backbone of a random copolymer 383 of NB and inactive spacer groups (Figure 5a). By assuming  $k_1$  384 =  $k_1^0 \times f$  and  $K_D^{-1} = K_D^{0-1} \times f$ , the optimized fits shown in Figure 385 5a, all based on an identical set of rate and equilibrium 386 constants (s = 10,  $k_1^0 = 0.12 \text{ M}^{-1} \text{ s}^{-1}$ ,  $K_D^0 = 0.026 \text{ M}$ , and  $k_r = 1$ 387 s<sup>-1</sup>), demonstrate an excellent agreement between the model 388 prediction and the experimental results with polymeric 389 initiators of four different chain grafting densities. In the 390 densely packed, brush-like macromolecular architecture, both 391 the rebinding and the colocalization effects are maximized to 392 facilitate a significantly increased local molarity between NCA 393 and active chain ends. Varying the grafting density provides a 394 direct means to regulate the kinetics by controlling the extent

of colocalization of active chains. This again suggests that the 395 strong auto-acceleration behavior is mainly due to the 396 enhanced binding interaction between NCA monomers and 397 the high density of actively growing chains in the brush. Figure 398 5b shows the model-predicted MWDs based on the estimated 399 rate constants and their comparison with the GPC measure- 400 ments (insets of Figure 5b and Table S3). Except for the 401 highest grafting density, the model agrees very well with the 402 experiments. In contrast, if we do not consider the binding step 403 explicitly in the propagation stage and use the phenomeno- 404 logical model<sup>23</sup> used in the original paper, although the kinetic 405 profiles can be fitted individually, the model would predict 406 MWs that significantly deviate from the GPC results (Figure 407 S5). The result show that a vast enhancement of the 408 polymerization rate can be induced by facilitating supra- 409 molecular interactions of reaction partners in a predefined 410 macromolecular architecture.

From single helices to "hinged" double helices and an array  $^{412}$  of helices attached on a polymeric backbone, the OMM model  $^{413}$  successfully described the kinetics of the ROP-NCA reactions  $^{414}$  with an almost identical  $k_{\rm r}$  and a  $K_{\rm D}$  that is varied by two to  $^{415}$  three magnitudes across different macromolecular structures.  $^{416}$  The difference in  $k_{\rm 1}$  may also be accounted for by a similar  $^{417}$  binding interaction between the monomer and active chains in  $^{418}$  the first growing stage. Altogether, the data suggests that the

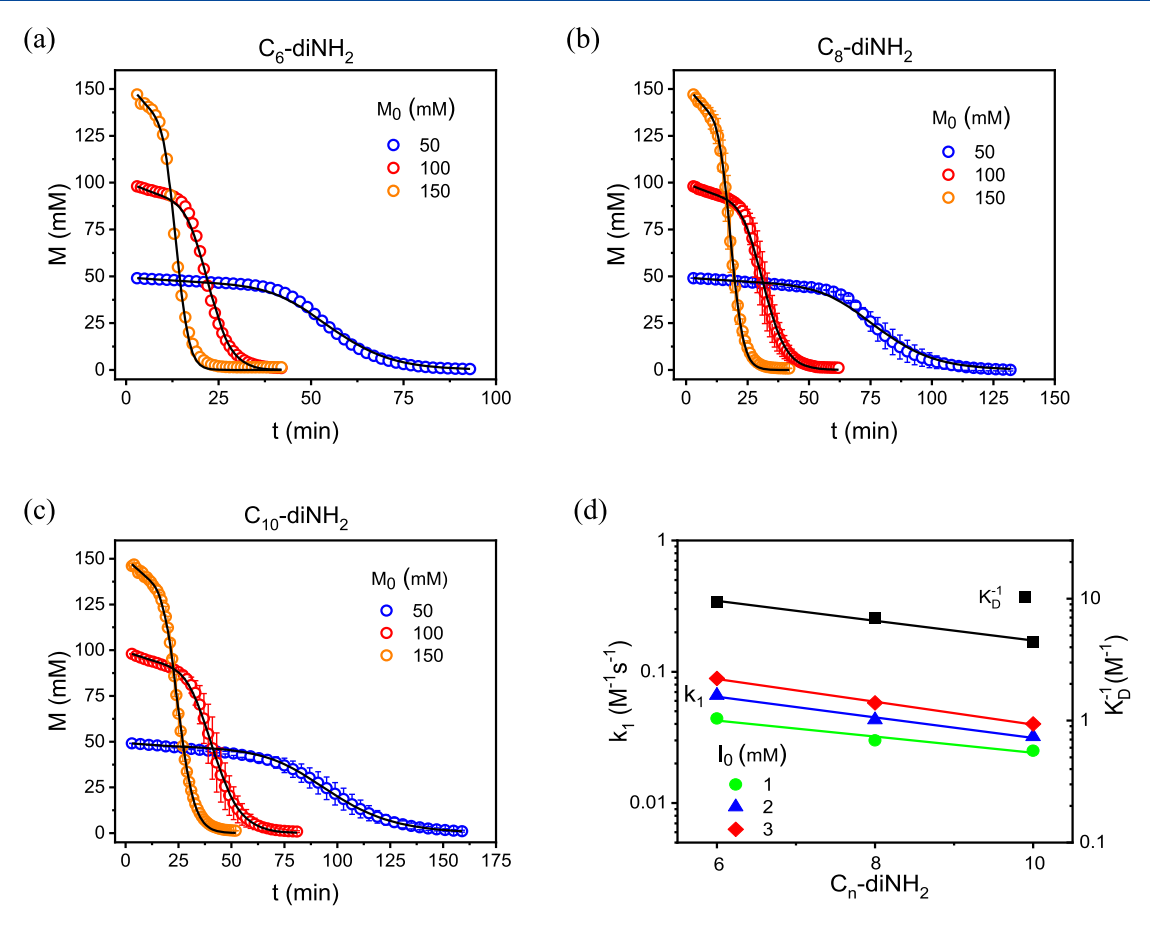


Figure 4. Analysis of polymerization of "hinged" helical polypeptides with the OMM model. (a–c). Kinetic data (circles) obtained from the polymerization of BLG-NCA in DCM using 1,6-diaminohexane ( $C_6$ -diNH<sub>2</sub>) (a), 1,8-diaminooctane ( $C_8$ -diNH<sub>2</sub>) (b), and 1,10-diaminodecane ( $C_{10}$ -diNH<sub>2</sub>) (c) as the initiator at  $M_0/I_0 = 50$ , and at selected value of  $M_0 = 50$ , 100, or 150 mM, respectively. Error bars represent standard deviations from three independent measurements at each condition. The nine sets of kinetic data are fit with the OMM model by sharing the same s and  $k_r$  globally (s = 10 and  $k_r = 1$  s<sup>-1</sup>) and the same  $K_D$  for each type of initiator, but allowing  $k_1$  to be individually optimized. (d) Extracted  $k_1$  and  $K_D^{-1}$  from (a–c) for different  $C_n$ -diNH<sub>2</sub>. The results show the dependence of the effective binding affinity of NCA to the helical chains on the spacer length, resulting from the proximity and colocalization of two active chains from the diamine initiators.

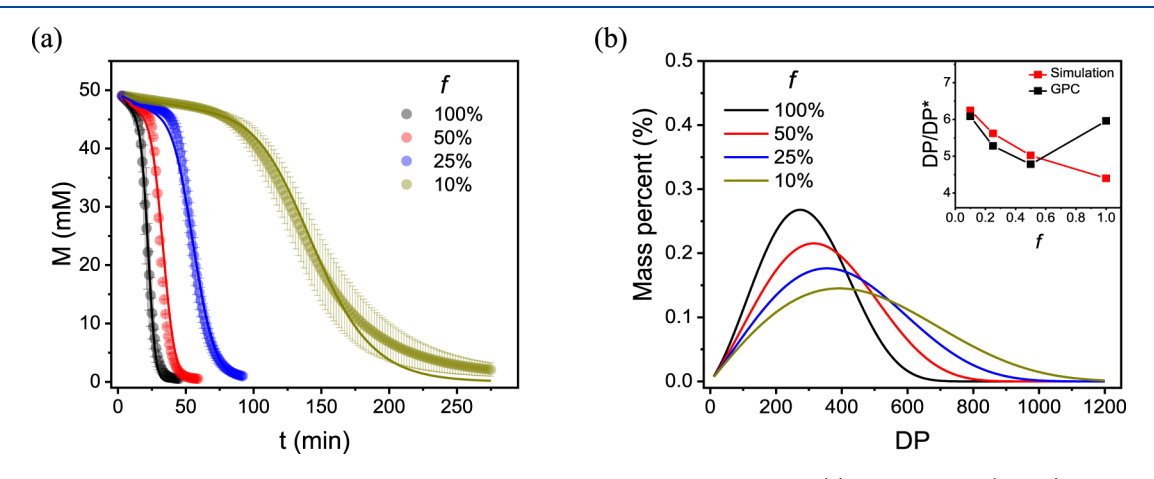


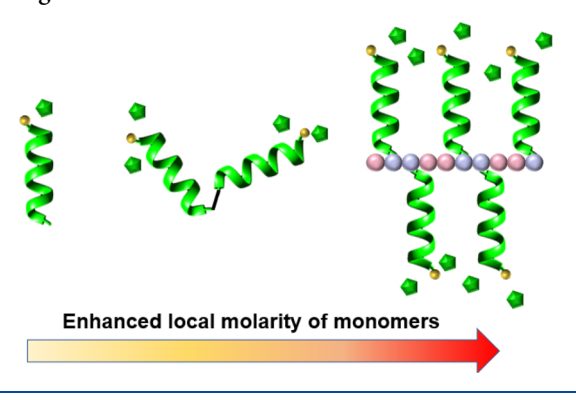
Figure 5. Analysis of "brush" polymerization of helical polypeptides with the OMM model. (a) Kinetic data (circles) obtained from the polymerization of BLG-NCA with random copolymer macroinitiators ( $M_0/I_0 = 50$ ) of varying densities of the initiating group (f = 10, 25, 50, and 100%) is fit with the OMM model (solid lines) globally at s = 10,  $k_1^0 = 0.12$  M $^{-1}$  s $^{-1}$ ,  $k_D^0 = 0.026$  M, and  $k_r = 1$  s $^{-1}$ . (b) Predicted MWD profiles based on the kinetic profiles in (a). Calculated DP (in red squares) at various f is compared to the GPC results (in black squares) in the inset. DP\* =  $M_0/I_0$  is used for normalization.

420 local enrichment of growing chains accomplished by the 421 macromolecular structures and the enhanced monomer 422 adsorption facilitated by the neighboring binding sites has a 423 profound effect on the effective binding strength of the growing chains and ultimately the catalytic nature of auto- 424 accelerated, cooperative covalent polymerizations (Scheme 2). 425 s2

Applicability of the Model for the Complex Reaction 426

Mechanism. Although the cooperative covalent polymer- 427

Scheme 2. Summary of Structural Effect on the Enhanced Binding



428 ization described here can be summarized using relatively 429 simple equations, other systems may present additional 430 complexity. For example, it is not unusual that additional 431 intermediates, covalent or noncovalent, occur in the reaction 432 pathway of actual chemical reactions, as schematically shown 433 in Figure 6a. To test whether the generalized OMM model still 434 holds for this complex mechanism, we first established the 435 corresponding concentration flux equations (Figure S6) from 436 the reaction scheme and simulated the kinetic profiles of 437 polymerization by the numerical method (Figure 6b). Then, 438 we examined whether the complete set of kinetic profiles (e.g., 439 starting from different  $M_0$ ) can still be described by the 440 generalized OMM model (eqs 2-6), in which  $K_D$  and  $k_r$  are 441 now replaced by  $K_{\rm M}$  and  $k_{\rm cat}$ . We found that, in most cases, the 442 generalized OMM model is a good approximation for the 443 cooperative covalent polymerization with hypothesized multi-444 ple intermediates, resulting in unique  $K_{
m M}$  and  $k_{
m cat}$  from the

fitting (Figure 6b, solid lines). We note that  $K_{\rm M}$  and  $k_{\rm cat}$  are 445 now combinations of various rate and equilibrium constants 446 and cannot be assigned to a particular molecular process. An 447 analogue to the MM parameters commonly used in enzymatic 448 reactions,  $K_{\rm M}$  should be regarded as an apparent dissociation 449 constant, and  $k_{\rm cat}$  as the apparent first order rate constant for 450 the chemical conversion. Figure 6c shows how the fitted  $K_{\rm M}$  451 and  $k_{\rm cat}$  are related with  $K_{\rm D}$  and  $k_{\rm T}$  used in the simulation of 452 kinetic profiles, respectively, when the equilibrium constant for 453 forming the second intermediate ( $K' = k_+/k_-$ ) varies by a few 454 orders in magnitude. By applying the steady-state assumption 455 to the intermediates, the apparent propagation rate constant in 456 the second stage can be derived and compared with the form 457 of the MM equation, resulting in a simple analytic equation of 458  $K_{\rm M}$  and  $k_{\rm cat}$  as

$$K_{\rm M} = \frac{k_{\rm p}k_{\rm r} + k_{\rm off}(k_{\rm -} + k_{\rm r})}{k_{\rm on}(k_{\rm +} + k_{\rm -} + k_{\rm r})} \approx \frac{K_{\rm D}}{1 + K'}$$

$$k_{\text{cat}} = \frac{k_{+}k_{\text{r}}}{k_{+} + k_{-} + k_{\text{r}}} \approx \frac{k_{\text{r}}}{1 + 1/K'}$$

when  $k_{\rm r}$  is relatively small. The solid lines in Figure 6c show 460 the prediction from the equations, in good agreement with the 461 fitting results obtained numerically at individual values of K'. 462

We provide another example in which the generalized OMM 463 model can accurately describe the covalent cooperative 464 polymerization in which a competitive side reaction occurs 465 in the accelerating stage (Supporting Information and Figures 466 S7, S8). As in the polymerization reaction, it is common for a 467 substrate molecule in the solution to bind in an alternative 468 unreactive mode at the active site of the growing chain. The 469 occurrence of such a competitive inhibition on the reaction 470

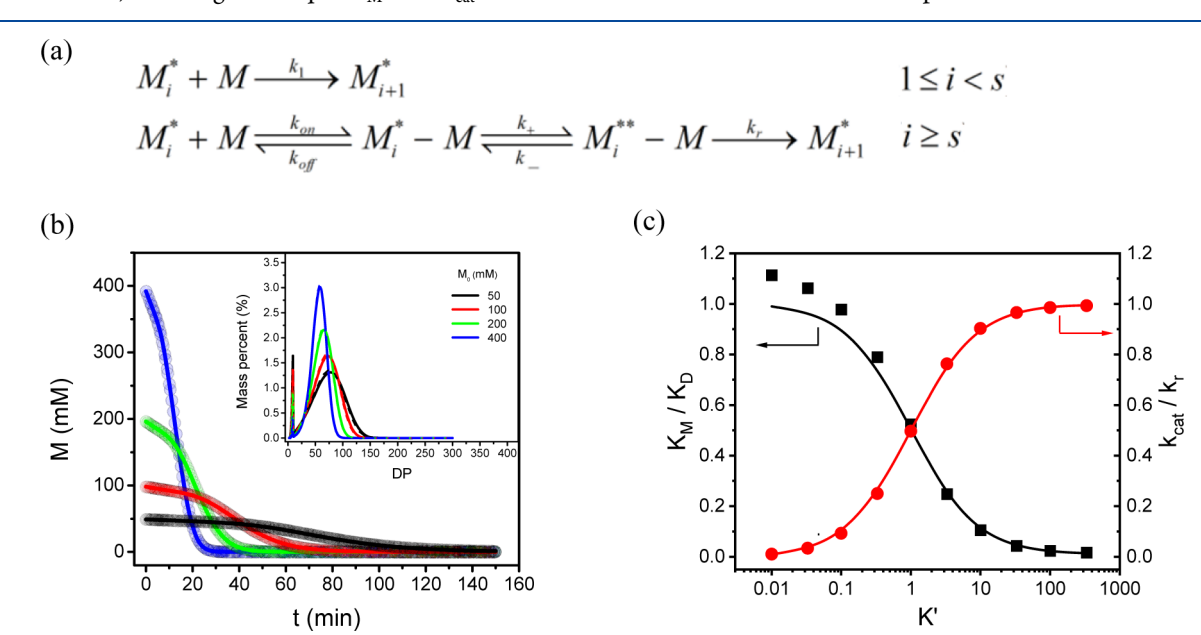


Figure 6. Validating the applicability of the OMM model for the complex reaction mechanism. (a) Reaction scheme for a case in which an additional intermediate occurs in the accelerating stage of cooperative covalent polymerization,  $k_+/k_-$  being the equilibrium constant (K') for forming the second intermediate. (b) Plots of the monomer concentration (in circles) vs time for test cases with s = 10,  $M_0/I_0 = 50$ ,  $k_1 = 0.05$  M $^{-1}$  s $^{-1}$ ,  $k_{\rm on} = 1 \times 10^3$  M $^{-1}$  s $^{-1}$ ,  $k_{\rm on} = 1 \times 10^2$  s $^{-1}$ ,  $k_{\rm on} = 1$ 

Macromolecules Article pubs.acs.org/Macromolecules

471 pathway can be examined in a similar way to that for multiple 472 intermediates. Again, the MM-like parameters in the OMM 473 model can be uniquely obtained from the kinetic profiles and 474 approximated by a simple analytic function of rate and 475 equilibrium constants, as long as the competitive inhibition is 476 not dominating the reaction. Reactions with even higher 477 complexity can be treated by combining the multiple 478 intermediates with the multiple competitive pathways.

The generalized OMM model should therefore provide a 480 practical solution to predict the overall kinetic behavior and 481 the MWD of resulting polymers and offer insightful 482 information on the reaction mechanism. It remains to be 483 seen to what extent the kinetic phenomena in novel systems 484 other than the ROP-NCA obey the generalized OMM model, 485 for all intents and purposes. It is reasonable to expect that, as 486 the MM equation holds for many enzymatic and catalytic 487 reactions, the OMM model should interpretate a variety of 488 cooperative covalent polymerizations in which noncovalent 489 interactions interplay with covalent interactions. The prototype 490 enzymatic behavior found in the auto-accelerated polymerization of helical polypeptides in varying macromolecular 492 architectures is likely not a coincidence, but due to the catalytic 493 nature of cooperative covalent polymerization in general and 494 the essential role of supramolecular binding interaction in this 495 type of polymerization reactions.

#### 496 CONCLUSIONS

497 The successful combination of the classical models of Oosawa 498 and MM has shown that artificial polymer systems can be 499 created in the likeness of complex biological systems. In this 500 work, we successfully modeled and demonstrated that a 501 synthetic polypeptide can behave as an "enzyme" by reversibly 502 binding and catalyzing a chemical reaction. In this case, 503 however, the polypeptide enzyme acts to catalyze a chemical 504 reaction that results in its own growth without any need for 505 specific amino acid side chains. Instead, this polymerization 506 relies on the structural features of the  $\alpha$ -helix to bind and 507 catalyze the polymerization, and the effect can be amplified by 508 increasing the local molarity of growing chains in the 509 proximity. This remarkable feature is so far unique to the 510 ROP, however, the model used to describe it can be leveraged 511 to identify other polymerizations with cooperative elements 512 and added complexity.

### ASSOCIATED CONTENT

#### 514 Supporting Information

517

518

519

520

521

522

523

524

525

526

527

528

529

515 The Supporting Information is available free of charge at 516 https://pubs.acs.org/doi/10.1021/acs.macromol.1c02606.

> Materials; instruments and characterization methods; experimental methods for polymerization kinetics; GPC characterization of resulting polypeptides; methods for kinetic modeling; description of the cooperative covalent polymerization model with a competitive side reaction; concentration flux kinetic equations; dimensionless form of the kinetic equations; analysis of the DPs of the resulting polymers; GPC light scattering traces for "hinged" polypeptides; simulation results for the cooperative covalent model with an inhibitive, competing side reaction; and detailed fitting results for homopolypeptides, "hinged" polypeptides, and "brush" polypeptides, and comparison with GPC analysis (PDF)

AUTHOR	INFORMATION	

#### **Corresponding Authors**

Jianjun Cheng - Department of Materials Science and Engineering and Department of Chemistry, University of Illinois at Urbana-Champaign, Urbana, Illinois 61801, *United States*; orcid.org/0000-0003-2561-9291; Email: jianjunc@illinois.edu

530

531

532

533

534

535

536

539

540

541

543

544

545

546

547

548

549

550

551

552

553

554

555

556

557

558

559

560

561

562

563

564

567

583

Yao Lin - Department of Chemistry and Polymer Program at 537 the Institute of Materials Science, University of Connecticut, 538 Storrs, Connecticut 06269, United States; o orcid.org/ 0000-0001-5227-2663; Email: yao.lin@uconn.edu

#### Authors

Hailin Fu – Department of Chemistry and Polymer Program 542 at the Institute of Materials Science, University of Connecticut, Storrs, Connecticut 06269, United States; orcid.org/0000-0002-3972-7659

Ryan Baumgartner – Department of Materials Science and Engineering and Department of Chemistry, University of Illinois at Urbana-Champaign, Urbana, Illinois 61801, United States

Ziyuan Song - Department of Materials Science and Engineering and Department of Chemistry, University of Illinois at Urbana-Champaign, Urbana, Illinois 61801, United States; orcid.org/0000-0002-3165-3712

Chongyi Chen - Department of Materials Science and Engineering and Department of Chemistry, University of Illinois at Urbana-Champaign, Urbana, Illinois 61801, United States

Complete contact information is available at: https://pubs.acs.org/10.1021/acs.macromol.1c02606

#### **Author Contributions**

§H.F., R.B., and Z.S. contributed equally.

The authors declare no competing financial interest.

#### **ACKNOWLEDGMENTS**

This work was supported by the NSF grant (DMR 1809497 to 565 Y.L. and CHE-1709820 to J.C.). 566

#### REFERENCES

- (1) Ramakrishnan, V. Ribosome structure and the mechanism of 568 translation. Cell 2002, 108, 557-572.
- (2) Sievers, A.; Beringer, M.; Rodnina, M. V.; Wolfenden, R. The 570 ribosome as an entropy trap. Proc. Natl. Acad. Sci. U.S.A. 2004, 101, 571 7897-7901.
- (3) Schmeing, T. M.; Ramakrishnan, V. What recent ribosome 573 structures have revealed about the mechanism of translation. Nature 574 2009, 461, 1234-1242.
- (4) Oosawa, F.; Kasai, M. A theory of linear and helical aggregations 576 of macromolecules. J. Mol. Biol. 1962, 4, 10-21.
- (5) Oosawa, F.; Asakura, S. Thermodynamics of the Polymerization of 578 Protein; Academic Press, 1975.
- (6) Kirschner, M.; Mitchison, T. Beyond self-assembly: From 580 microtubules to morphogenesis. Cell 1986, 45, 329-342.
- (7) Lüders, J.; Stearns, T. Microtubule-organizing centres: a re- 582 evaluation. Nat. Rev. Mol. Cell Biol. 2007, 8, 161-167.
- (8) Dominguez, R.; Holmes, K. C. Actin structure and function. 584 Annu. Rev. Biophys. 2011, 40, 169-186.
- (9) Kuriyan, J.; Eisenberg, D. The origin of protein interactions and 586 allostery in colocalization. Nature 2007, 450, 983-990. 587
- (10) Pawson, T.; Scott, J. D. Signaling Through Scaffold, Anchoring, 588 and Adaptor Proteins. Science 1997, 278, 2075-2080.

ı

- 590 (11) Mueller, A.; O'Brien, D. F. Supramolecular materials via 591 polymerization of mesophases of hydrated amphiphiles. *Chem. Rev.* 592 **2002**, *102*, 727–758.
- 593 (12) Ciferri, A. Supramolecular polymerizations. *Macromol. Rapid* 594 *Commun.* **2002**, 23, 511–529.
- 595 (13) Zhao, D.; Moore, J. S. Nucleation-elongation: A mechanism for 596 cooperative supramolecular polymerization. *Org. Biomol. Chem.* **2003**, 597 1, 3471–3491.
- 598 (14) Zhong, S.; Cui, H.; Chen, Z.; Wooley, K. L.; Pochan, D. J. Helix 599 self-assembly through the coiling of cylindrical micelles. *Soft Matter* 600 **2007**, *4*, 90–93.
- 601 (15) De Greef, T. F. A.; Smulders, M. M. J.; Wolffs, M.; Schenning, 602 A. P. H. J.; Sijbesma, R. P.; Meijer, E. W. Supramolecular 603 polymerization. *Chem. Rev.* **2009**, *109*, 5687–5754.
- 604 (16) Aida, T.; Meijer, E. W.; Stupp, S. I. Functional supramolecular 605 polymers. *Science* **2012**, *335*, 813–817.
- 606 (17) Ogi, S.; Sugiyasu, K.; Manna, S.; Samitsu, S.; Takeuchi, M. 607 Living supramolecular polymerization realized through a biomimetic 608 approach. *Nat. Chem.* **2014**, *6*, 188–195.
- 609 (18) Kang, J.; Miyajima, D.; Mori, T.; Inoue, Y.; Itoh, Y.; Aida, T. A 610 rational strategy for the realization of chain-growth supramolecular 611 polymerization. *Science* **2015**, *347*, 646–651.
- 612 (19) Lutz, J.-F.; Lehn, J.-M.; Meijer, E. W.; Matyjaszewski, K. From 613 precision polymers to complex materials and systems. *Nat. Rev. Mater.* 614 **2016**, *1*, 16024.
- 615 (20) Sorrenti, A.; Leira-Iglesias, J.; Markvoort, A. J.; De Greef, T. F. 616 A.; Hermans, T. M. Non-equilibrium supramolecular polymerization. 617 *Chem. Soc. Rev.* **2017**, *46*, 5476–5490.
- 618 (21) Wehner, M.; Würthner, F. Supramolecular polymerization 619 through kinetic pathway control and living chain growth. *Nat. Rev.* 620 *Chem.* 2020, 4, 38–53.
- 621 (22) Hashim, P. K.; Bergueiro, J.; Meijer, E. W.; Aida, T. 622 Supramolecular Polymerization: A Conceptual Expansion for 623 Innovative Materials. *Prog. Polym. Sci.* **2020**, *105*, 101250.
- 624 (23) Baumgartner, R.; Fu, H.; Song, Z.; Lin, Y.; Cheng, J. 625 Cooperative polymerization of  $\alpha$ -helices induced by macromolecular 626 architecture. *Nat. Chem.* **2017**, *9*, 614–622.
- 627 (24) Chen, C.; Fu, H.; Baumgartner, R.; Song, Z.; Lin, Y.; Cheng, J. 628 Proximity-Induced Cooperative Polymerization in "Hinged" Helical 629 Polypeptides. *J. Am. Chem. Soc.* **2019**, *141*, 8680–8683.
- 630 (25) Song, Z.; Fu, H.; Wang, J.; Hui, J.; Xue, T.; Pacheco, L. A.; Yan, 631 H.; Baumgartner, R.; Wang, Z.; Xia, Y.; Wang, X.; Yin, L.; Chen, C.; 632 Rodríguez-López, J.; Ferguson, A. L.; Lin, Y.; Cheng, J. Synthesis of 633 polypeptides via bioinspired polymerization of in situ purified N-634 carboxyanhydrides. *Proc. Natl. Acad. Sci. U.S.A.* **2019**, *116*, 10658–635 10663.
- 636 (26) Song, Z.; Fu, H.; Baumgartner, R.; Zhu, L.; Shih, K.-C.; Xia, Y.; 637 Zheng, X.; Yin, L.; Chipot, C.; Lin, Y.; Cheng, J. Enzyme-mimetic self-638 catalyzed polymerization of polypeptide helices. *Nat. Commun.* **2019**, 639 *10*, 5470.
- 640 (27) Doty, P.; Lundberg, R. D. Polypeptides. X. Configurational and 641 stereochemical effects in the amine-initiated polymerization of N-642 carboxyanhydrides. *J. Am. Chem. Soc.* **1956**, *78*, 4810–4812.
- 643 (28) Lundberg, R. D.; Doty, P. Polypeptides. XVII. A study of the 644 kinetics of the primary amine-initiated polymerization of N-carboxy-645 anhydrides with special reference to configurational and stereo-646 chemical effects. *J. Am. Chem. Soc.* **1957**, *79*, 3961–3972.
- 647 (29) Ballard, D. G. H.; Bamford, C. H.; Elliott, A. Synthetic 648 polypeptides. *Macromol. Chem. Phys.* **1960**, 35, 222–238.
- 649 (30) Michaelis, L.; Menten, M. Die kinetik der invertinwirkung. 650 *Biochem. J.* **1913**, *Z49*, 333–369.
- 651 (31) Dear, A. J.; Meisl, G.; Michaels, T. C. T.; Zimmermann, M. R.;
- 652 Linse, S.; Knowles, T. P. J. The catalytic nature of protein aggregation. 653 *J. Chem. Phys.* **2020**, *152*, 045101.
- 654 (32) Fersht, A. Structure and Mechanism in Protein Science: A Guide to 655 Enzyme Catalysis and Protein Folding; Macmillan, 1999.
- 656 (33) Briggs, G. E.; Haldane, J. B. S. A Note on the Kinetics of 657 Enzyme Action. *Biochem. J.* **1925**, *19*, 338–339.